Novel Airborne Polarimetry Retrievals as Constraints on Drop Size Distributions in Aerosol-Aware Large-Eddy Simulations and a Foundational Framework for Use of Space-based Retrievals to Evaluate Earth System Models

COLUMBIA CLIMATE SCHOOL
CENTER FOR CLIMATE SYSTEMS RESEARCH

McKenna W. Stanford, Ann M. Fridlind, Andrew S. Ackerman, Bastiaan van Diedenhoven, Qian Xiao, Jian Wang, Toshihisa Matsui, Daniel Hernandez-Deckers, and Paul Lawson

Introduction & Motivation

- Cloud drop size distributions (DSDs) modulate precipitation formation, cold pools, & the vertical profiles of droplet number concentration (N_d) and effective radius (R_{eff})
- DSD evolution is influenced by (but not limited to):
  1. Aerosol particle size distribution (PSD) profile
  2. Collision-coalescence
  3. Entrainment & dilution
- The airborne Research Scanning Polarimeter (RSP) provides retrievals of cloud-top N_d & R_{eff} that complements in situ observations for constraining high-resolution simulations
- The RSP was deployed during the NASA Cloud, Aerosol, and Monsoon Processes Philippines Experiment (CAMP^{2}Ex; Reid et al., 2023) field campaign (2019) & provided retrievals in the cumulus congestus regime

Objectives:

1. Utilize RSP cloud-top retrievals & in situ cloud microphysics & aerosol measurements to constrain large eddy simulations (LES) of cumulus congestus
2. Determine factors controlling the vertical profile of N_d & R_{eff}
3. Demonstrate foundational framework for using polarimetric retrievals to constrain simulations that can translate to recently launched space-borne polarimeters and Earth system models (ESMs)
4. Employ thermal tracking framework to obtain process-level understanding of DSD evolution at the source of droplet production

Data & Methods

Research Scanning Polarimeter (RSP)

- Retrieval of cloud droplet size from polarized observations of the reflected light in the rainbow region (scattering angles between 135° and 165°) based on structure of cloud bow
- RSP yields: **(1)** accurate retrieval of R_{eff} and **(2)** novel characterization of DSD width via effective variance (V_{eff}); Both R_{eff} and V_{eff} → N_d ***at cloud top***

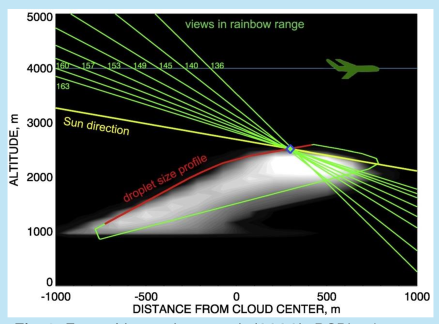

Fig.1. From Alexandrov et al. (2020). RSP's view-lines forming the polarized rainbow for a point at the cloud surface.

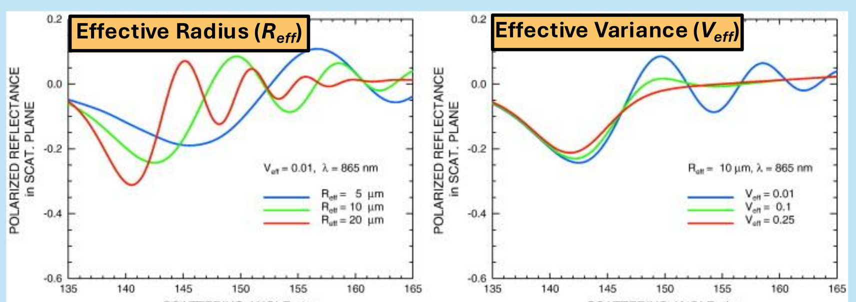

Fig.2. From Alexandrov et al. (2012). Structure of polarized reflectance in the rainbow angular range and sensitivity to the effective radius (left) and effective variance (right) of the DSD.

In Situ Aerosol & Cloud Measurements

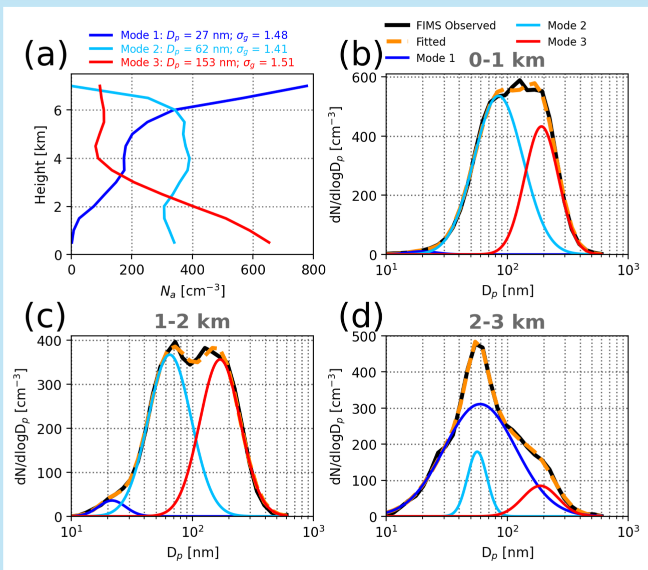

Fig.3. From Stanford et al. (2020). (a) Profiles of N_a for 3 lognormal modes. (b)-(d) Lognormal aerosol PSDs for three example altitude ranges that span sub-cloud to upper entrainment environments.

- Aerosol PSDs measured by Fast Integrated Mobility Spectrometer (FIMS; Wang et al., 2017) are used to derive trimodal, lognormal PSDs w/ height-invariant aerosol number concentration (N_a) & height-varying geometric mean particle diameter (D_p) and geometric standard deviation (σ_g) for simulation initialization
- Cloud probes onboard the SPEC, Inc. Learjet used to construct DSDs in warm regions of congestus

Large Eddy Simulations

Model Description & Setup

- **Model:** Distributed Hydrodynamic Aerosol and Radiative Modeling for Atmospheres (DHARMA; Ackerman et al. 2000)
- **Δx:** 100 m
- **Δz:** 20-100 m (finer in BL)
- **Domain Size:** 19.2 x 19.2 km
- **Boundary Conditions:** Doubly Periodic
- **Microphysics:** Bulk (2M based on Morrison et al., 2009) & Bin (CARMA; Ackerman et al., 1995)
- **For simplicity:** No radiation or ice
- **Large-scale conditions:** Thermodynamics & vertical motion harvested from NU-WRF (Peters-Lidard et al., 2015) mesoscale simulations

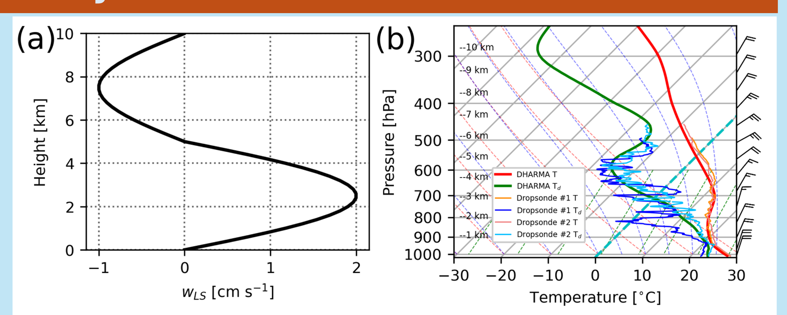

Fig.4. From Stanford et al. (2020). Profiles of (a) large-scale vertical motion (w_{LS}) and (b) thermodynamic profiles shown on a skew T – log P diagram from the NU-WRF-derived sounding & 2 dropsondes released by aircraft.

Sensitivity Tests

Simulation Name	Description
CNTL	Seifert and Beheng (2001) warm-rain formulation
NO_AC	As in CNTL, w/ autoconversion turned off
FIXED_AERO	As in CNTL, w/ aerosol PSD fixed to cloud-base value for entire profile
2X_AC	As in CNTL, w/ autoconversion scaled by a factor of 2
KK	Khairoutdinov and Kogan (2000) warm-rain formulation
FIXED_AERO_NO_AC	As in CNTL, w/ autoconversion turned off AND fixed aerosol PSD to cloud-base value
BIN	Size-resolved bin microphysics
BIN_TURB	As in BIN, w/ turbulent enhancement of collision-coalescence
BIN_TURB_10X	As in BIN_TURB, w/ turbulent enhancement scaled by a factor of 10

Results

(1) Cloud Droplet Evolution

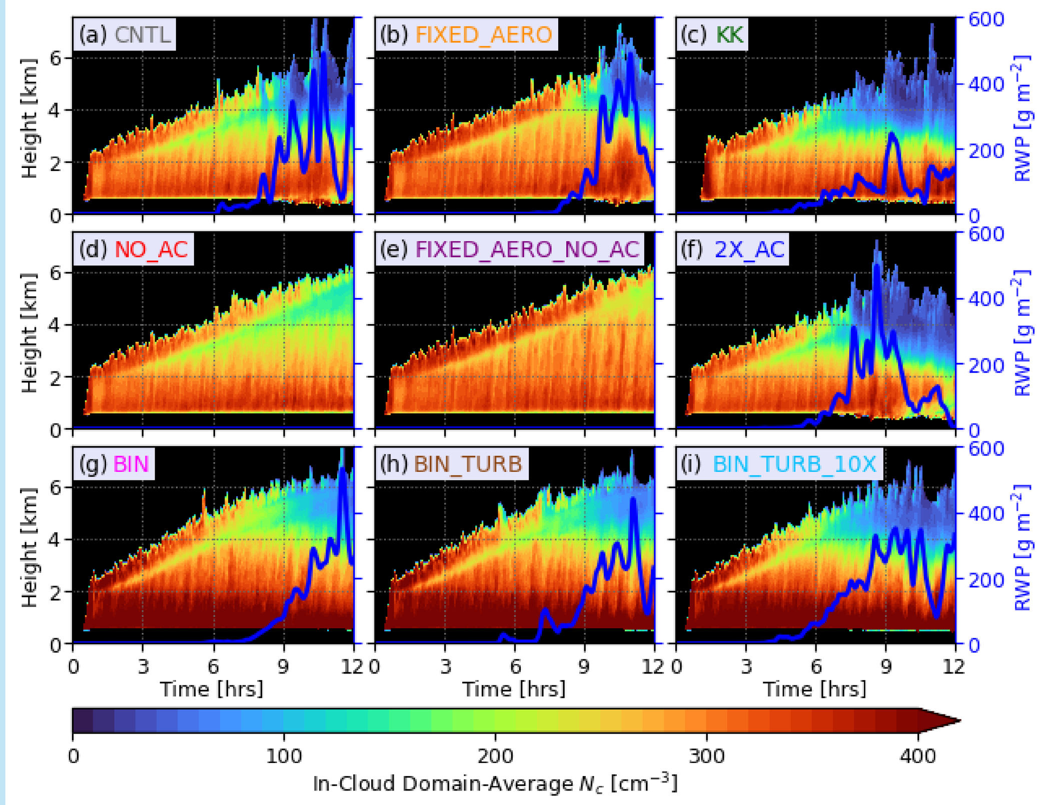

Fig.5. From Stanford et al. (2024). Time-height series of in-cloud domain average cloud droplet number concentration (N_c) for all simulations. Blue lines (right ordinates) show the rain water path (RWP) time series.

Key Points

- Autoconversion/collision-coalescence decreases cloud droplet number concentration (N_c) with altitude
- Neglecting height variation in N_a profile leads to greater N_c with height

(2) N_d & R_{eff} Comparison w/ RSP & in situ

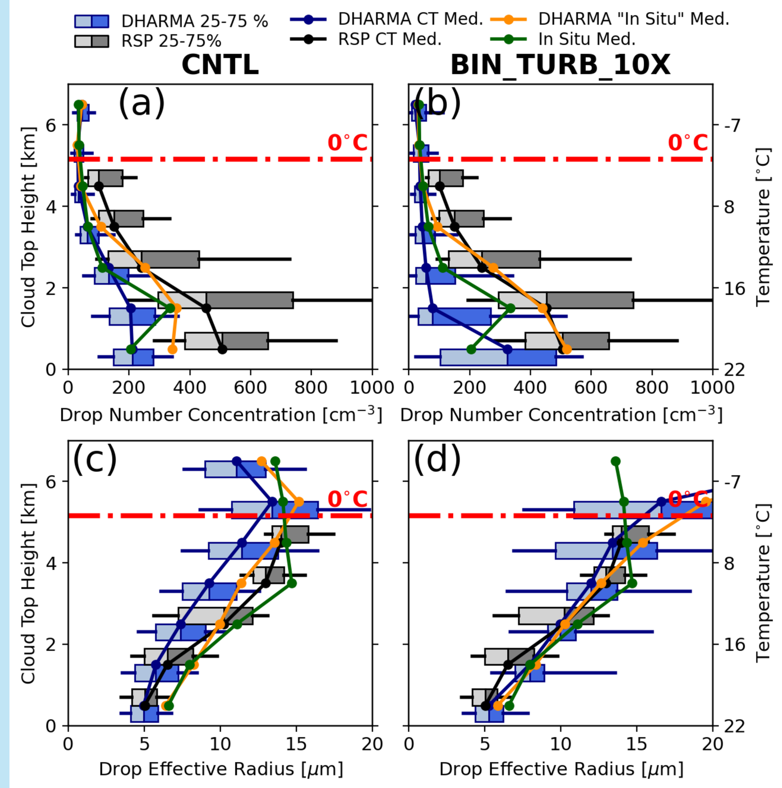

Fig.6. From Stanford et al. (2024). Profile distributions for DHARMA & RSP cloud-top values (blues & greys, respectively) of N_d (top row) & R_{eff} (bottom row). Median profiles for observed in situ values and simulated "in situ" values are shown as green & orange lines, respectively.

Key Points

- Both simulations present low bias in N_d but appropriately decrease N_d w/ height
- Both simulations appropriately increase R_{eff} with height; BIN_TURB_10X matches RSP well, but CNTL low-biased

(3) Comparing Simulated vs. Observed DSDs

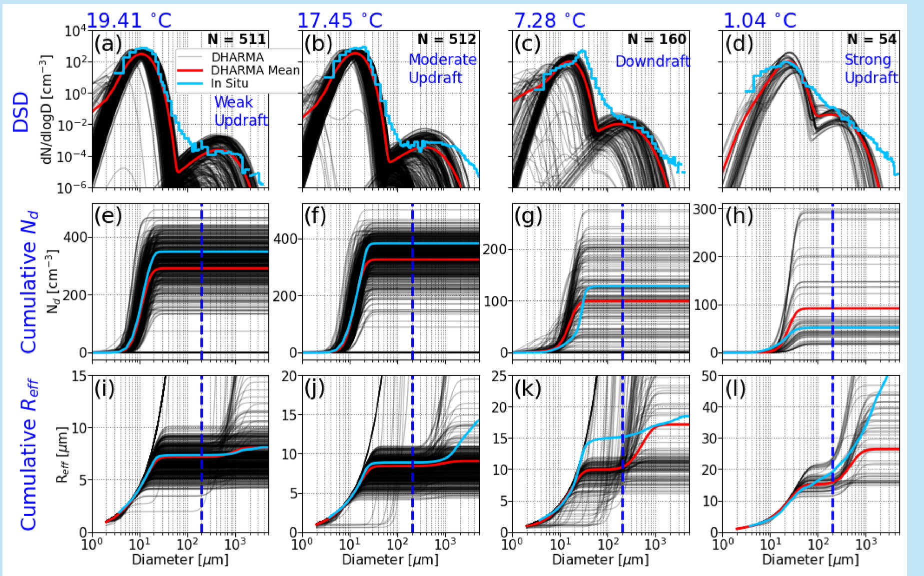

Fig. 7. From Stanford et al. (2024). (a)-(d) Averaged "cloud pass" DSDs at various temperature levels (warmer to colder from left to right) in various dynamic conditions for the CNTL simulation. (e)-(f) Cumulatively integrated N_d for each cloud pass. (i)-(l) Cumulatively integrated R_{eff} for each cloud pass.

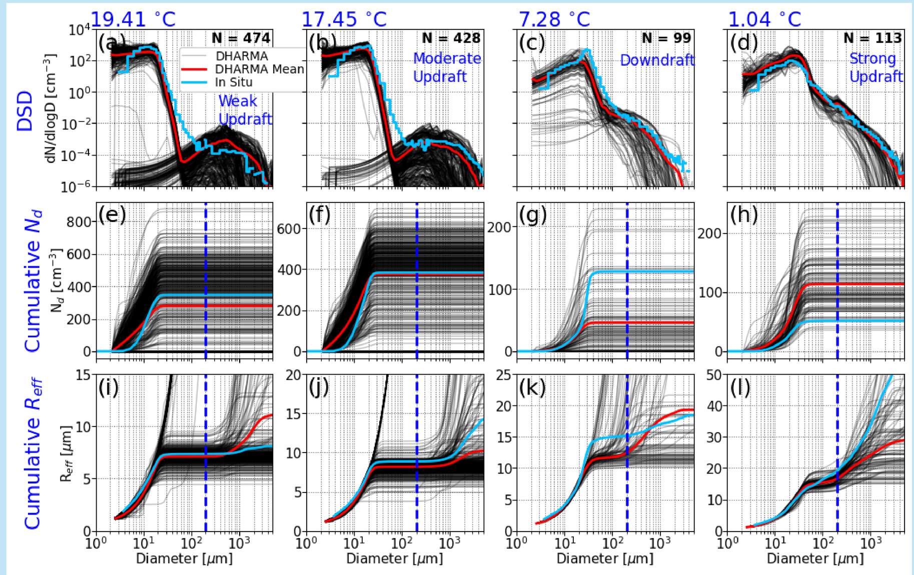

Fig. 8. From Stanford et al. (2024). As in Fig. 7 but for the BIN_TURB_10X simulation.

Key Points

- Both simulations appropriately show broadening of DSD with height (decreasing temperature) and capture cloud & precipitation modes
- Cumulatively integrated N_d & R_{eff} show N_d is sensitive to narrow range of sizes & simulations capture clustering around observed values

(4) Thermal-Tracking Framework

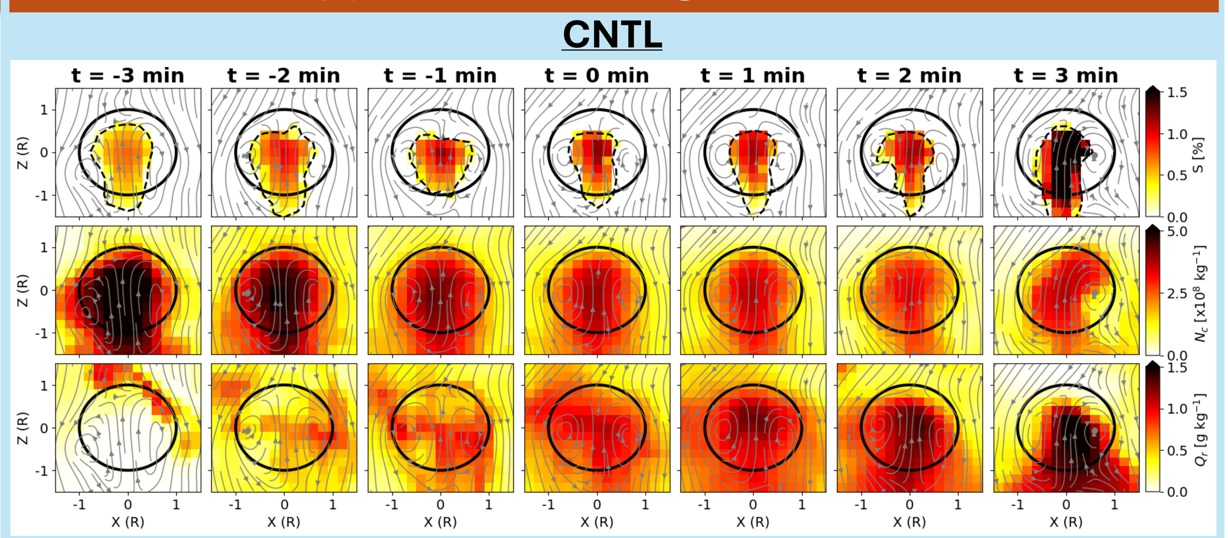

Fig.9. From Stanford et al. (2024). Thermal composite evolution in X-Z plane for supersaturation (S; top row), cloud droplet number concentration (N_c; middle row), & rain mass mixing ratio (Q_r; bottom row) for the CNTL simulation. Composites are centered (t = 0 min) around max. ascent rate.

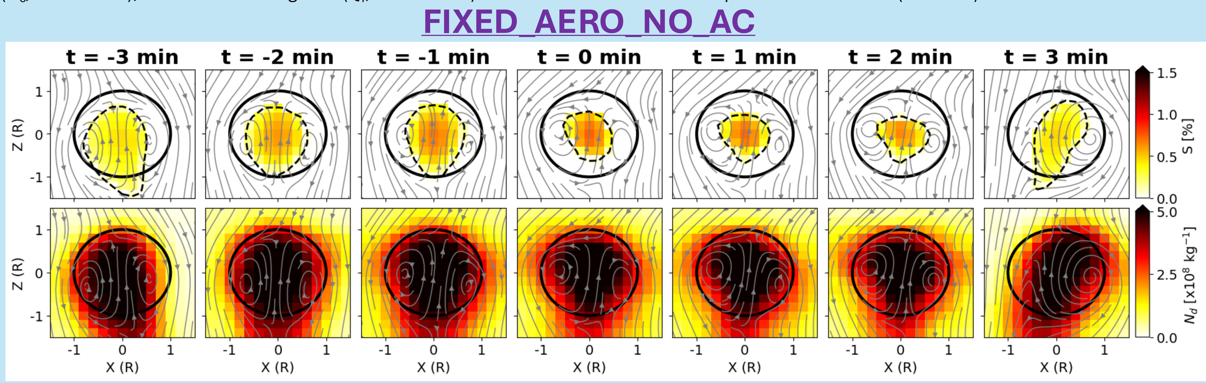

Fig.10. From Stanford et al. (2024). As in Fig. 9 but for the FIXED_AERO_NO_AC simulation, excluding Q_r since autoconversion is neglected.

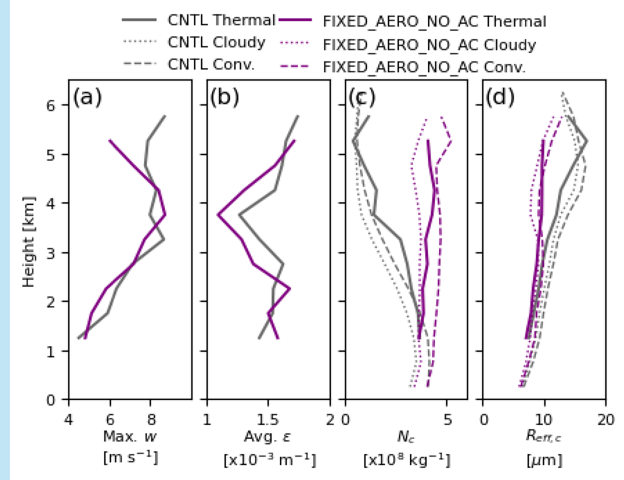

Fig.11. From Stanford et al. (2024). Average thermal profiles for CNTL & FIXED_AERO_NO_AC simulations of (a) max. vertical velocity (w), (b) avg. fractional entrainment rate (ε), (c) avg. N_c, & (d) avg. cloud droplet R_{eff}.

Tracking Methodology

- Tracking algorithm developed by Hernandez-Deckers and Sherwood (2016)
- One-minute output for last 3 hrs of CNTL & FIXED_AERO_NO_AC simulations; the latter chosen to investigate role of height-varying N_a and autoconversion on diluting N_d (i.e., isolating entrainment)
- Narrows focus of cloud droplet production to source mechanisms in rising thermals
- Explicitly calculates fractional entrainment rate ($\boldsymbol{\varepsilon}$)

Key Points

- CNTL simulation experiences substantial dilution of N_c throughout thermal lifetime
- Neglecting autoconversion & height-varying N_a (FIXED_AERO_NO_AC) leads to no significant dilution of N_c through thermal lifetime, despite comparable average entrainment rates ($\boldsymbol{\varepsilon}$) and maximum vertical velocity (w) as in CNTL
- Average thermal profiles show a constant profile of N_c with height for the FIXED_AERO_NO_AC simulation in units kg^{-1} (i.e., controlling for dilution via expansion)
  - Averaging over cloudy (LWC > 0.1 g kg-1) or convective cloudy (LWC > 0.1 g kg^{-1} & w > 1 m s^{-1}) grid points results in same constant profile (Fig. 11, dashed & dotted lines)
  - Suggests that without these 2 factors, the role of entrainment in diluting N_c is offset by continuous (secondary) activation (likely via toroidal circulations)

Translation to Space

PACE Mission

- PACE successfully launched on 8 Feb. 2024 w/ two polarimeters
- Combined, SPEXone & HARP2 provide retrievals of aerosol absorption & composition, cloud droplet sizes, and ice particle shapes & roughness
- Translating RSP studies to space-borne platforms presents a unique set of challenges (see below)

SPEXone (Spectro-polarimeter for Planetary Exploration) [SRON]

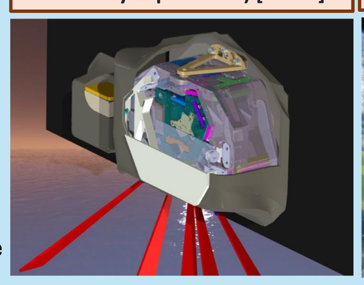

HARP2 (Hyper-Angular Rainbow Polarimeter #2) [UMBC]

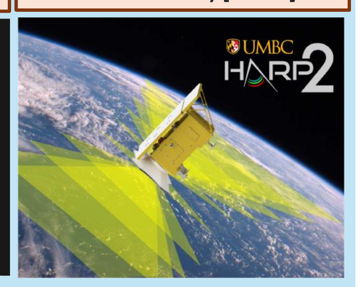

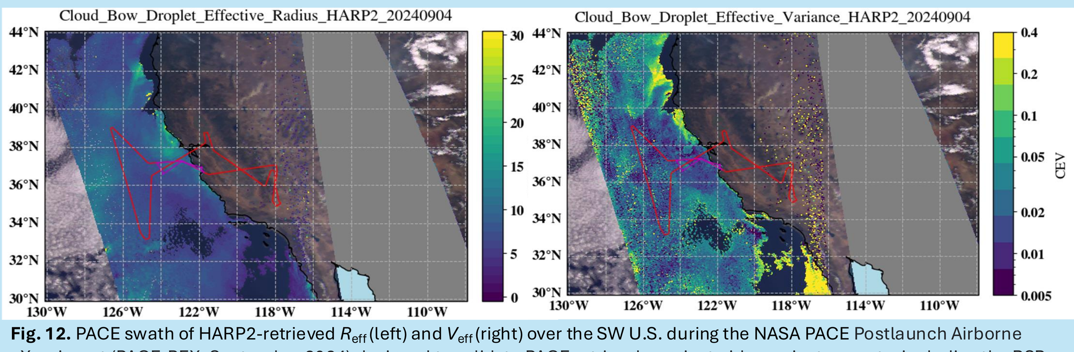

Fig. 12. PACE swath of HARP2-retrieved R_{eff} (left) and V_{eff} (right) over the SW U.S. during the NASA PACE Postlaunch Airborne eXperiment (PACE-PEX; September 2024) designed to validate PACE retrievals against airborne instruments, including the RSP. The red lines indicate the flight path of the NASA ER-2 aircraft housing the RSP. Figure courtesy of Chamara Rajapakshe (NASA GSFC). Data courtesy of the PACE and PACE-PAX teams.

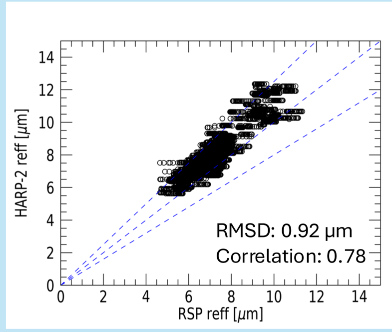

Fig. 13. Comparison of HARP2 vs. RSP R_{eff} during the flight shown in Fig. 12.). Data courtesy of the PACE and PACE-PAX teams.

	RSP	HARP-2	SPEXone
UV-NIR range (bandwidth)	410, 470, 550, 670, 865, 960, 1590, 1880, & 2260 nm	440, 550, 670, & 870 nm	Continuous from 385 to 770 nm in 2-4 nm steps
Ground Footprint	~ 120 m (depends on aircraft speed)	3 km	2.5 km
Swath Width	± 60˚	± 47˚ (1556 km at nadir)	± 4˚ (100 km at nadir)
Number of Viewing Angles	152 at 0.8˚ increments	10 for 440, 550, and 870 nm & 60 for 670 nm (spaced over 114˚)	5 (-57˚, -20˚, 0˚, 20˚, 57˚)
Global Coverage	N/A	2 days	~ 30 days

Adapted from Werdell et al. (2019), showing instrument specifications of polarimeters on PACE and compared to those of the airborne RSP.

Uniqueness & Challenges

- Polarimeters provide improved R_{eff} retrievals over bi-spectral methods (Fu et al., 2022) and novel information on DSD width via V_{eff} retrievals
- Space-borne polarimeters have much larger footprint than RSP
- Need to develop simulators (*à la* COSP, EMC^2) for subcolumn variability representation and appropriate cloud-top retrieval emulation in ESM evaluations
- Validation of N_d assumptions for various cloud regimes

Conclusions

- RSP retrievals of cloud-top N_d & R_{eff} were used to complement in situ measurements to constrain LES of a cumulus congestus case during the NASA field campaign CAMP^{2}Ex
- Both bulk and bin microphysics schemes appropriately reproduce RSP trend of decreasing N_d & increasing R_{eff} with increasing CTH, but both schemes produce a low bias in N_d (compared to RSP) while the bin scheme reproduces R_{eff} magnitudes well
- Thermal-based analysis shows that in the absence of autoconversion (collision-coalescence) & a height-varying N_a profile, the role of entrainment in diluting N_d is offset by continuous (secondary) activation in thermals
- New space-borne polarimeters on the PACE mission will provide global coverage of polarimetric retrievals to constrain cloud microphysical properties in ESMs, but present unique challenges associated with much larger footprints & need for simulator development

References

Ackerman, A. S., Hobbs, P. V., and Toon, O. B.: A Model for Particle Microphysics, Turbulent Mixing, and Radiative Transfer in the Stratocumulus-Topped Marine Boundary Layer and Comparisons with Measurements, Journal of Atmospheric Sciences, 52, 1204 – 1236, https://doi.org/10.1175/1520-0469(1995)0522.0.CO;2, 1995.

Ackerman, A. S., Toon, O. B., Stevens, D. E., Heymsfield, A. J., Ramanathan, V., and Welton, E. J.: Reduction of Tropical Cloudiness by Soot, Science, 288, 1042–1047, https://doi.org/10.1126/SCIENCE.288.5468.1042, 2000.

Alexandrov, M. D., Cairns, B., Emde, C., Ackerman, A. S., and van Diedenhoven, B.: Accuracy assessments of cloud droplet size retrievals from polarized reflectance measurements by the research scanning polarimeter, Remote Sensing of Environment, 125, 92–111, https://doi.org/10.1016/J.RSE.2012.07.012, 2012.

Alexandrov, M.D., D.J. Miller, C. Rajapakshe, A. Fridlind, B. van Diedenhoven, B. Cairns, A.S. Ackerman, and Z. Zhang: Vertical profiles of droplet size distributions derived from cloud-side observations by the Research Scanning Polarimeter: Tests on simulated data. *Atmos. Res.*, **239**, 104924, doi:10.1016/j.atmosres.2020.104924, 2020.

Cairns, B., Russell, E. E., and Travis, L. D.: Research Scanning Polarimeter: calibration and ground-based measurements, In *Polarization: Measurement, Analysis, and Remote Sensing II, 18 Jul. 1999, Denver, Col.*, Proc. SPIE, vol. 3754, p. 186, https://doi.org/10.1117/12.366329, 1999.

Fu, D., Di Girolamo, L., Rauber, R. M., McFarquhar, G. M., Nesbitt, S. W., Loveridge, J., Hong, Y., Van Diedenhoven, B., Cairns, B., Alexandrov, M. D., Lawson, P., Woods, S., Tanelli, S., Schmidt, S., Hostetler, C., and Scarino, A. J.: An evaluation of the liquid cloud droplet effective radius derived from MODIS, airborne remote sensing, and in situ measurements from CAMP2Ex, Atmospheric Chemistry and Physics, 22, 8259–8285, https://doi.org/10.5194/ACP-22-8259-2022, 2022.

Hernandez-Deckers, D. and Sherwood, S. C.: A Numerical Investigation of Cumulus Thermals, Journal of the Atmospheric Sciences, 73, 4117–4136, https://doi.org/10.1175/JAS-D-15-0385.1, 2016.

Khairoutdinov, M. and Kogan, Y.: A New Cloud Physics Parameterization in a Large-Eddy Simulation Model of Marine Stratocumulus, Monthly Weather Review, 128, 229 – 243, https://doi.org/10.1175/1520-0493(2000)1282.0.CO;2, 2000.

Morrison, H., Thompson, G., and Tatarskii, V.: Impact of Cloud Microphysics on the Development of Trailing Stratiform Precipitation in a Simulated Squall Line: Comparison of One- and Two-Moment Schemes, Monthly Weather Review, 137, 991–1007, https://doi.org/10.1175/2008MWR2556.1, 2009.

Peters-Lidard, C. D., Kemp, E. M., Matsui, T., Santanello, J. A., Kumar, S. V., Jacob, J. P., Clune, T., Tao, W. K., Chin, M., Hou, A., Case, J. L., Kim, D., Kim, K. M., Lau, W., Liu, Y., Shi, J., Starr, D., Tan, Q., Tao, Z., Zaitchik, B. F., Zavodsky, B., Zhang, S. Q., and Zupanski, M.: Integrated modeling of aerosol, cloud, precipitation and land processes at satellite-resolved scales, Environmental Modelling & Software, 67, 149–159, https://doi.org/10.1016/J.ENVSOFT.2015.01.007, 2015.

Reid, J. S. et al. : The coupling between tropical meteorology, aerosol lifecycle, convection, and radiation, during the Cloud, Aerosol and Monsoon Processes Philippines Experiment (CAMP2Ex), Bulletin of the American Meteorological Society, -1, https://doi.org/10.1175/BAMS-D-21-0285.1, 2023.

Seifert, A. and Beheng, K. D.: A double-moment parameterization for simulating autoconversion, accretion and selfcollection, Atmospheric Research, 59-60, 265–281, https://doi.org/10.1016/S0169-8095(01)00126-0, 2001.

Stanford, M., Fridlind, A., Ackerman, A., van Diedenhoven, B., Xiao, Q., Wang, J., Matsui, T., Hernandez-Deckers, D., and Lawson, P.: Warm-phase Microphysical Evolution in Large Eddy Simulations of Tropical Cumulus Congestus: Constraining Drop Size Distribution Evolution using Polarimetery Retrievals and a Thermal-Based Framework, EGUsphere [preprint], https://doi.org/10.5194/egusphere-2024-2413, 2024.

Wang, J., Pikridas, M., Spielman, S. R., and Pinterich, T.: A fast integrated mobility spectrometer for rapid measurement of sub-micrometer aerosol size distribution, Part I: Design and model evaluation, Journal of Aerosol Science, 108, 44–55, https://doi.org/10.1016/J.JAEROSCI.2017.02.012, 2017.

Werdell, P. J., Behrenfeld, M. J., Bontempi, P. S., Boss, E., Cairns, B., Davis, G. T., Franz, B. A., Gliese, U. B., Gorman, E. T., Hasekamp, O., Knobelspiesse, K. D., Mannino, A., Martins, J. V., McClain, C., Meister, G., and Remer, L. A.: The plankton, aerosol, cloud, ocean ecosystem mission status, science, advances, Bulletin of the American Meteorological Society, 100, 1775–1794, https://doi.org/10.1175/BAMSD-18-0056.1, 2019.

Pacific Northwest NATIONAL LABORATORY
PNNL is operated by Battelle for the U.S. Department of Energy
BATTELLE
U.S. DEPARTMENT OF ENERGY
SRON Netherlands Institute for Space Research
UNIVERSIDAD NACIONAL DE COLOMBIA
EARTH SYSTEM SCIENCE INTERDISCIPLINARY CENTER